The 4th European sCO_2 Conference for Energy Systems
March 23-24, 2021, Online Conference

2021-sCO2.eu-103

EXPERIMENTAL INVESTIGATIONS ON THE HEAT TRANSFER CHARACTERISTICS OF SUPERCRITICAL CO_2 IN HEATED HORIZONTAL PIPES

Konstantinos Theologou*
M. Sc.
Institute of Nuclear Technology and Energy Systems (IKE), University of Stuttgart
Stuttgart, Germany
Email: konstantinos.theologou@ike.uni-stuttgart.de

Rainer Mertz
Dr.-Ing.
Institute of Nuclear Technology and Energy Systems (IKE), University of Stuttgart
Stuttgart, Germany

Eckart Laurien
Prof. Dr.-Ing.
Institute of Nuclear Technology and Energy Systems (IKE), University of Stuttgart
Stuttgart, Germany

Jörg Starflinger
Prof. Dr.-Ing.
Institute of Nuclear Technology and Energy Systems (IKE), University of Stuttgart
Stuttgart, Germany

ABSTRACT

In the frame of the sCO_2-QA (**q**ualification of **a**nalysis tools for the evaluation of a residual heat-driven, self-sufficient system for decay heat removal) project, a residual heat-driven self-sufficient sCO_2-operated decay heat removal system based on a Brayton cycle is simulated with the German thermal-hydraulics system code ATHLET (**a**nalysis of **th**ermal-hydraulics of **le**aks and **t**ransients). The heat removal system consists of a compact heat exchanger in the containment, a turbo-compressor system located in the reactor building and a gas cooler in the outdoor area. The validation of ATHLET and other numerical codes as well as understanding the heat transfer characteristics of sCO_2 near the critical point requires experimental data. At IKE (Institute of Nuclear Technology and Energy Systems), the SCARLETT (**s**upercritical **c**arbon **d**ioxide **l**oop at IKE Stuttgart) test facility is available for various experiments with sCO_2.

This publication includes an experimental investigation of the thermal stratification in heated horizontal sCO_2 pipe flows. For this investigation, eight test series with overall 48 experiments were carried out in two pipes with inner diameters of 4 mm and 8 mm. The experiments were carried out at a pressure of approximately 7.75 MPa. The target values of mass flux were set at 400 kg/m^{2}s and 800 kg/m^{2}s and those of heat flux at 50, 90 and 130 kW/m^2, resulting in a heat to mass flux ratio of 62.5-225 J/kg. The inlet Reynolds numbers are between 16000 and 120000. The measured parameters are the flow rate, the pressure, the inlet and outlet fluid temperature as well as the outer surface temperature along the test pipe in three different radial angles.

The results show the influence of the pipe diameter, Reynolds number, mass and heat flux on the temperature stratification. Also, inflow lengths were determined for a fully developed temperature stratification. This data set can be used for the validation of computer codes.

INTRODUCTION

Since the accidents in the boiling water reactors in Fukushima Daiichi in 2011, the reliable decay heat removal came into the focus of reactor safety research of nuclear power plants. This gave reason to create a new concept of a heat removal system. The concept of a residual heat-driven self-sufficient sCO_2-operated decay heat removal system is based on a simple Brayton cycle which was simulated with the German thermal hydraulics system code ATHLET [1]. Figure 1 shows a conceptual sketch of a boiling water reactor (BWR) with one decay heat removal system. The three main components of the sCO_2-operated decay heat removal system are a compact heat exchanger (CHX) located in the reactor containment, a turbo-compressor system (TCS) in the reactor building and a gas cooler located in the outdoor area. The CHX has to be compact because of space limitations in the containment. Driven by natural convection of the steam-cycle in the containment the sCO_2 is heated up inside the CHX and flows through a turbine to the gas cooler where the decay heat is transferred to an ultimate heat sink, e.g. the ambient air. Downstream, the compressor of the

* corresponding author(s)

DOI: 10.17185/duepublico/73945

TCS compresses the sCO_2 again. The turbine generates more energy than needed by the compressor so excess electrical energy generated by the generator can be used for different purposes, e.g. for charging the batteries of the power plant.

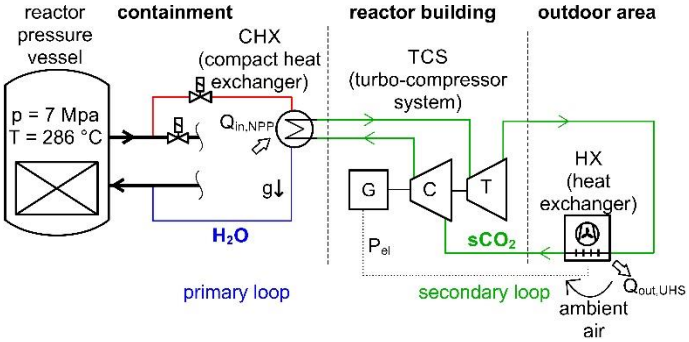

Figure 1: sCO_2-operated decay heat removal system

The simulation of the cycle with ATHLET by Venker [1] showed the general feasibility of such a concept. However, the comparison of the calculated and the existing experimental data show large deviations in the area of the compressor inlet where the CO_2 is close to the critical point. The reason for this fact is that ATHLET uses correlations for heat transfer and pressure drop which are valid for constant fluid properties and not validated for the operation near the critical point. When using sCO_2 as working fluid these correlations have to be validated with experimental data due to non-constant fluid properties. While a lot of research is available for vertical pipes, there is a lack of experimental data for horizontal pipe flows. For this purpose, basic investigations on heated horizontal pipes are carried out first.

Direct Numerical Simulations (DNS) were carried out by Chu [2] for heated sCO_2 pipe flow with 1 mm and 2 mm inner diameter. The results show that buoyancy leads to a non-uniform distribution of wall temperature in the circumferential direction of the pipe. The results are limited to an inlet Reynolds number of 5400 due to the high computational effort of DNS. In the simulations, the variable fluid properties near the critical point lead to a temperature and density stratification in the horizontal flow direction. The fluid with the lower density is in the upper part of the cross-section and the fluid with the higher density is in the lower part. Experimental data for horizontal sCO_2 pipe flows can be found under cooling conditions by Dang and Hihara [3], Liao and Zhao [4] and Wahl et al. [5]. Other researchers investigate the heat transfer of sCO_2 in horizontal cooled pipes numerically [6–10].

Yu et al. [11] investigated the heat transfer of supercritical water in horizontal heated pipes with inner diameters of 26 mm and 43 mm experimentally and numerically and showed the effect of heat transfer deterioration on the top surface of the test pipe while an enhanced heat transfer occurs at the bottom surface. They considered the temperature difference between the top and the bottom of the test pipes as a measure for buoyancy effects in horizontal flows. This stratification effect disappeared with smaller pipe diameter. Bazargan and Fraser [12] presented a new numerical model and a new experimental correlation for horizontal heated pipe flows of supercritical water and compared them with experimental data of a pipe with an internal diameter of 6.42 mm. The new correlation and the experiments are in good agreement but they found a lack of experimental data for horizontal supercritical fluid flows with buoyancy effects to evaluate models and empirical correlations.

EXPERIMENTAL SETUP AND METHODS

Experimental investigations of the heat transfer characteristics of sCO_2 are carried out in horizontal heated pipes with constant heat flux. Temperatures are measured on the top surface, on the bottom surface and on the side of the pipe to investigate effects of temperature stratification for parameters close to the critical point. The inner diameters of the pipes are 4 mm and 8 mm with inlet Reynolds numbers of 16000 to 120000.

The above-mentioned experiments are performed using the test facility SCARLETT. It was built at IKE and is in operation since 2016. SCARLETT is a supercritical CO_2 loop in which different test rigs can be implemented modularly. Figure 2 displays a simplified scheme of the test facility.

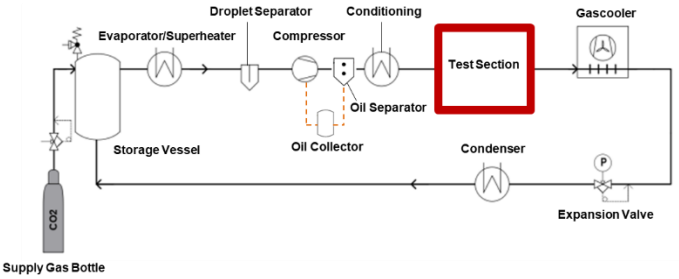

Figure 2: Simplified scheme of the test facility SCARLETT

Starting from the storage vessel the CO_2 flows into the evaporator where it will be overheated. A droplet separator guarantees that the piston compressor does not suck liquid CO_2. Downstream of the compressor an oil recirculation system with an over-dimensioned coalescence separator extracts more than 99 % of the compressor lubricant and brings it back to the compressor. The oil-concentration of the sCO_2 in the test section was investigated experimentally and is less than 0.2 m%. During conditioning, the sCO_2 can be heated with a flow heater or cooled with cryostats depending on the purpose of the experiment. At the entrance of the modular test section, SCARLETT provides the CO_2 under defined conditions: Pressures between 7.5 MPa and 12 MPa, temperatures between 5 °C and 150 °C and mass flows between 0.013 kg/s and 0.111 kg/s. After leaving the test section, a gas cooler cools down the sCO_2. The expansion valve expands the sCO_2 into the two-phase region. A condenser liquefies the wet steam completely before it flows back to the storage vessel. For more detailed information about the SCARLETT see Flaig et al. [13].

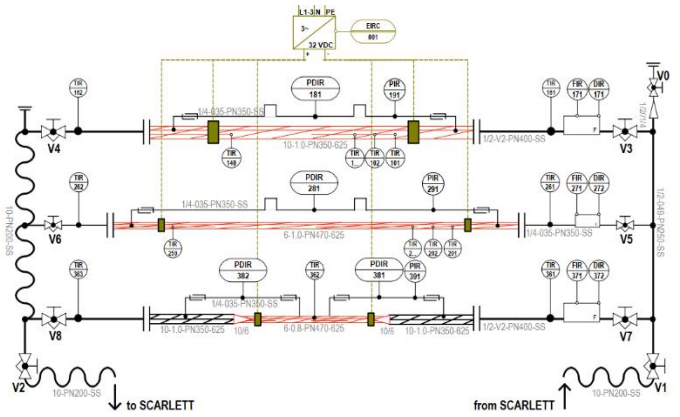

Figure 3: P&I Diagram of the test rig

For fundamental investigations of the heat transfer characteristics and pressure drop of sCO_2 near the critical point a new test rig was build up at IKE (Figure 3). The test rig consists of three tubular test sections with different pipe diameters. By bypassing the sCO_2 through the pipes, the mass flow can be adjusted. The test rig is variably mounted on a rack allowing experiments with horizontal, upward and downward mass flows. The first and the second test section have the same structure; the only difference is the inner diameter of the used test pipes (4 mm and 8 mm). The third pipe is used as a bypass of sCO_2 to adjust the mass flux through the other two test sections. The test pipes are heated up directly with a DC power supply. To insulate the test rig electrically from the test pipes special insulating flanges are used. The test sections were also thermally insulated with the synthetic high-temperature rubber "Armaflex". At the entrance of the test pipes, the mass flows and the bulk temperatures of sCO_2 are measured using Coriolis mass flowmeters with an accuracy of ±0.19 % of full scale and PT100 resistance temperature sensors with a Class A accuracy ±(0,15+0,002•T RD). Figure 4 shows the dimensions of the test pipes with an inner diameter of 4 mm and 8 mm for the presented experiments.

The total length of the first test pipe is 2360 mm with a heated length of 1640 mm. The second test pipe is 2500 mm long with a heated length of 2040 mm. Forty temperature sensors are tied with a temperature resistant yarn straight in line in 40 mm distances on the outer surface of the first test pipe and fifty sensors on the second test pipe. By rotating the pipe axially in 90° increments three times and repeating the experiments with the same parameter configuration, three surface temperature profiles of the horizontal flow direction can be measured: The horizontal temperature profile for the pipe bottom (HB), the pipe top (HT) and the pipe side (HM). The sensors are surface thin-film resistance temperature sensors (PT100) with a Class A accuracy. The absolute pressure is measured in front of the heated area and the differential pressure is measured over the heated length. To measure the pressure inside the test pipe without influencing the flow a 1 mm hole has been drilled into the pipe wall. The accuracy of the differential and absolute pressure transmitters is ±0.15 % of full scale. With the inner pipe diameter d_i, the unheated hydraulic inflow length L_{hyd} for a hydraulic fully developed flow has been calculated with the empirical formula of Munson [14] for a turbulent flow on the maximum expected Reynolds number.

$$\frac{L_{hyd}}{d_i} = 4.4Re^{\frac{1}{6}} \quad (1)$$

Alloy 625 was chosen for the pipe material because of its high specific electrical resistance. The inner roughness of the 4 mm pipe is Ra= 0,549 µm and Ra= 0,227 µm for the 8 mm pipe. The electrical power heating up the test pipes is measured directly at the DC power supply terminals to avoid voltage losses in the over-dimensioned copper terminals. The monitoring accuracy of the DC power supply is given with ±0.2 % of full scale.

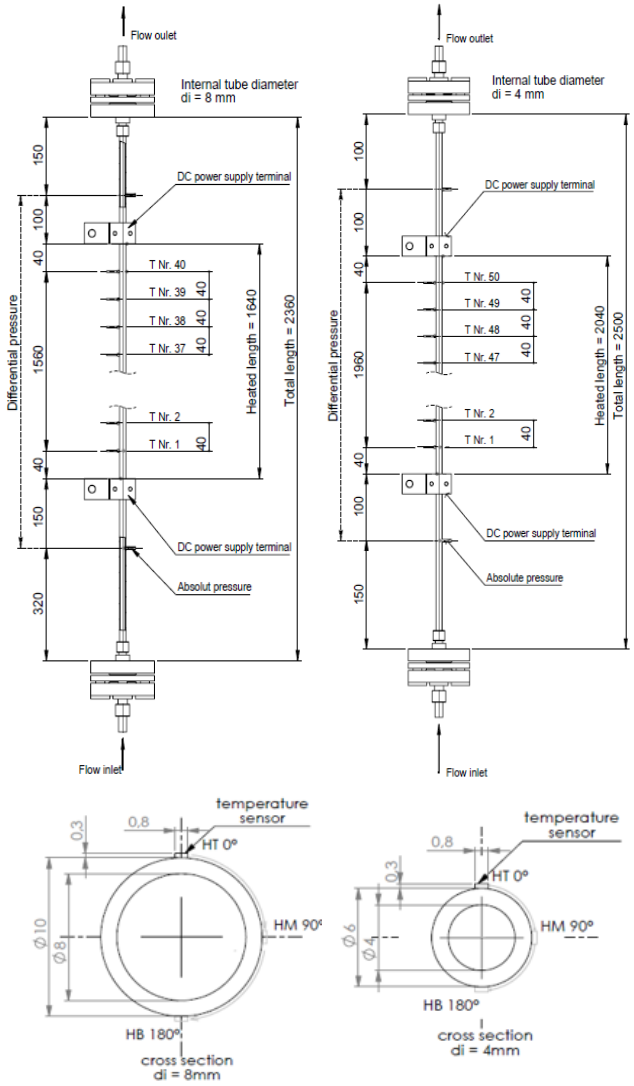

Figure 4: Dimensions of the 1st (left) and 2nd (right) test section

For the data acquisition, twenty-minute intervals with a 0.25 Hz recording frequency were selected. The arithmetic mean for each parameter was calculated using approximately 300 values. To ensure the reproducibility of the measurement some experiments were repeated two or three times. All experiments start after having reached steady-state conditions. To verify adiabatic conditions during the experiments the energy balance of the measured thermal and electrical heat flow was calculated with the transferred heat $\dot{Q}$, the mass flux $\dot{m}$, the specific enthalpy i, the electrical power P, the voltage U and the electrical current I:

$$|\dot{Q}_{el}| = |\dot{Q}_{th}| = \dot{Q} \quad (2)$$

$$\dot{Q}_{th} = \dot{m} * [i_{b,out}(T_{B,out}, p_{out}) - i_{b,in}(T_{B,in}, p_{in})] \quad (3)$$

$$\dot{Q}_{el} = P_{el} = U * I \quad (4)$$

For the detailed calculation of the heat transfer coefficient (htc) see Theologou et al. [15].

The following table gives an overview of the experimental parameters of the presented experiments.

Table 1: Experimental parameters

Parameter	Unit	Value
inner pipe diameter	mm	4, 8
flow orientation	-	horizontal
position of temperature sensors	-	HT (0 °), HM (90 °), HB (180 °)
inlet pressure	MPa	7.75
inlet temperature	°C	5, 20, 25, 30
mass flux	kg/m^{2}s	400, 800
heat flux	kW/m^2	50, 90, 130
inlet Reynolds numbers	-	16000-120000

RESULTS AND DISCUSSION

For the experimental investigation of the thermal stratification in heated horizontal sCO_2 pipe flows, eight test series (TS) were carried out with overall 48 experiments. Table 2 shows an overview of the actual values: the inner pipe diameter d_i, the inlet temperature of the bulk fluid $T_{b,in}$, the mass flux G, the heat flux $\dot{q}$, the absolute inlet pressure p_{in}, the pressure drop over the heated length Δp, the inlet Reynolds number Re_{in}, the heat loss (equation 2-4) and the arithmetic mean of the relative error for the heat transfer coefficient $\overline{s_h}$ with the standard deviation σ_h. Within each TS, there are constant target values of the mass flux, the heat flux and the absolute inlet pressure. By axial rotation of the pipes, the outer surface temperatures can be measured at the three sensor positions (SP) HB, HM and HT. To be able to provide a temperature profile over a larger enthalpy range the inlet temperature of the fluid is varied.

The results are presented in eight Figures (Figure 5-Figure 12) which include two charts for each TS. In the left charts, the inner wall temperature profile is plotted over the bulk enthalpy and in the right charts, the local htc is plotted over the bulk enthalpy. Also, in the left-hand diagrams, the bulk fluid temperature is plotted in grey for a constant pressure of 7.75 MPa. The dotted black lines in the figures represent the bulk fluid temperature and enthalpy at the pseudocritical point also for of pressure of 7.75 MPa. In the captions, the target value of the fluid inlet temperature and the position of the temperature sensors is described. The sensor positions on the top of the pipe surface is coloured red, green for the side and blue for the bottom surface. Experiments with higher inlet temperatures are coloured darker. The distance between two data points (DP) on the test pipe is 40 mm (Figure 4). This enables the determination of the inflow length which is necessary for the formation of the temperature stratification by counting the data points (1 DP = 40 mm = 10d).

Table 2 shows the heat losses ($1 - |\dot{Q}_{th}/\dot{Q}_{el}|$). To calculate the heat losses, an enthalpy balance is presented in equation 2. If, however, the measured fluid outlet temperature is close to the pseudocritical temperature, this calculation is highly erroneous and may be unsuitable for determining the heat losses. This case occurs in some experiments in TS4, TS6 and TS7. Additionally, table 2 also shows the arithmetic mean of the relative error of the htc and the standard deviation. For the calculation of the local error of the inner wall temperature, the most relevant parameter is the accuracy of the PT100 ±(0,15+0,002•T RD). Further errors in this error calculation are the accuracy of the specification of the thermal conductivity of the pipe material and the accuracy of the diameter specification. Due to the fixed part of the PT100 accuracy, the maximum relative error always occurs at the first surface PT100 with the lowest temperature. The absolute error increases with increasing temperature and is in the measured range of the 4 mm pipe approximately ±0.24 °C at 25 °C and ±0.34 °C at 120 °C. For the 8 mm pipe, it is approximately ±0.26 °C at 35 °C and ±0.50 °C at 160 °C. The maximum relative (and the minimum absolute) error of the bulk fluid enthalpy is at the inlet of the test section with the fluid inlet temperature as the major influencing parameter. Further errors in this error calculation are the accuracies of the mass flow meter and the pressure sensor. For the experiments with a fluid inlet temperature of approximately 5 °C the maximum relative error is 0.8 % and for the experiments with a fluid inlet temperature of approximately 30 °C the maximum relative error is 1.6 %.

Table 2: Experimental overview

TS	d_i [mm]	SP	$T_{b,in}$ [$°C$]	$G\left[\frac{kg}{m^2 s}\right]$	$\dot{q}\left[\frac{kW}{m^2}\right]$	p_{in} [MPa]	Δp [kPa]	Re_{in} [$-$]	$1 - \lvert\dot{Q}_{th}/\dot{Q}_{el}\rvert$ [%]	$\overline{s_h}$ [%]	σ_h [%]
TS1	4	HB	7.1	420	51.0	7.73	5.11	17040	1.5	2.7	0.6
			20.2	417	51.1	7.77	4.31	21943	2.8	3.0	1.0
		HM	7.3	414	51.0	7.74	4.73	16868	1.4	2.4	0.6
			20.1	417	51.1	7.78	5.24	21895	1.5	2.7	1.0
		HT	5.4	424	51.0	7.74	5.16	16702	2.5	2.1	0.6
			20.0	415	51.1	7.76	4.32	21728	3.5	2.5	1.1
TS2	4	HB	6.6	819	51.0	7.74	6.74	32911	3.5	5.9	1.2
			25.1	810	51.0	7.76	8.05	48627	0.9	6.3	2.9
		HM	6.4	820	50.9	7.74	6.45	32873	2.6	5.5	1.1
			24.4	821	51.0	7.73	7.69	48372	1.9	5.7	2.2
		HT	4.9	834	50.9	7.74	6.59	32581	4.1	4.9	1.0
			24.8	833	51.0	7.74	8.17	49651	0.3	5.2	2.7
TS3	4	HB	6.5	813	91.7	7.76	10.62	32620	0.3	2.8	1.1
			20.2	810	91.8	7.78	11.64	42592	0.7	2.6	0.6
		HM	6.7	819	91.7	7.73	10.48	33024	0.1	2.7	1.1
			20.0	832	91.7	7.79	12.07	43594	0.4	2.5	0.6
		HT	5.0	817	91.7	7.75	10.30	31937	0.3	2.1	0.7
			19.9	856	91.7	7.77	12.05	44728	0.4	2.3	0.6
TS4	8	HB	6.5	411	50.4	7.71	2.44	33532	13.4	3.2	0.5
			25.1	405	50.4	7.71	1.29	49495	13.5	2.3	0.5
		HM	4.9	401	50.4	7.76	1.07	31811	11.1	2.2	0.5
			25.2	401	50.4	7.74	1.22	49022	13.1	1.7	0.5
		HT	6.4	400	50.4	7.71	2.46	32551	18.1	1.4	0.4
			25.0	403	50.4	7.69	1.16	49230	12.8	1.1	0.3
TS5	8	HB	6.5	405	89.8	7.71	3.00	33016	1.4	1.1	0.2
			20.1	405	89.8	7.74	2.43	43151	0.2	1.2	0.2
		HM	7.0	398	89.8	7.77	3.08	32754	1.3	0.9	0.1
			19.9	404	89.3	7.76	1.75	42897	0.1	0.9	0.2
		HT	6.5	401	89.8	7.72	2.78	32677	0.9	0.7	0.1
			19.9	406	89.8	7.71	2.40	43148	1.0	0.7	0.1
TS6	8	HB	20.0	802	50.2	7.73	2.66	85370	3.7	8.2	1.3
			29.7	793	50.3	7.70	2.96	116302	33.3	7.2	3.0
		HM	19.9	816	50.3	7.77	2.98	86568	3.6	7.1	0.9
			29.6	795	50.3	7.72	2.83	115525	33.2	6.0	3.1
		HT	19.9	798	50.3	7.73	2.58	84844	4.3	5.9	1.0
			30.0	796	50.3	7.79	2.93	117029	27.2	4.5	3.5
TS7	8	HB	6.5	801	90.3	7.72	3.30	65290	5.8	4.5	1.0
			20.0	793	90.2	7.77	3.12	84322	15.3	3.1	0.4
			29.7	807	90.2	7.71	3.16	118406	6.2	2.5	0.3
		HM	7.6	796	90.3	7.78	3.35	66165	6.7	3.9	0.5
			19.9	800	90.2	7.78	2.76	84967	15.8	2.6	0.5
			29.8	810	90.2	7.72	3.18	118826	5.5	2.0	0.5
		HT	6.2	800	90.3	7.74	3.57	64833	5.4	2.2	0.6
			19.9	798	90.2	7.73	2.62	84836	16.9	1.5	0.5
			30.1	790	90.2	7.78	3.12	116490	4.4	1.4	0.6
TS8	8	HB	6.5	799	130.4	7.73	3.42	65165	10.8	1.5	0.1
		HM	7.2	801	130.4	7.80	3.60	65990	9.5	1.2	0.2
		HT	6.2	810	130.4	7.74	3.71	65652	11.6	0.9	0.2

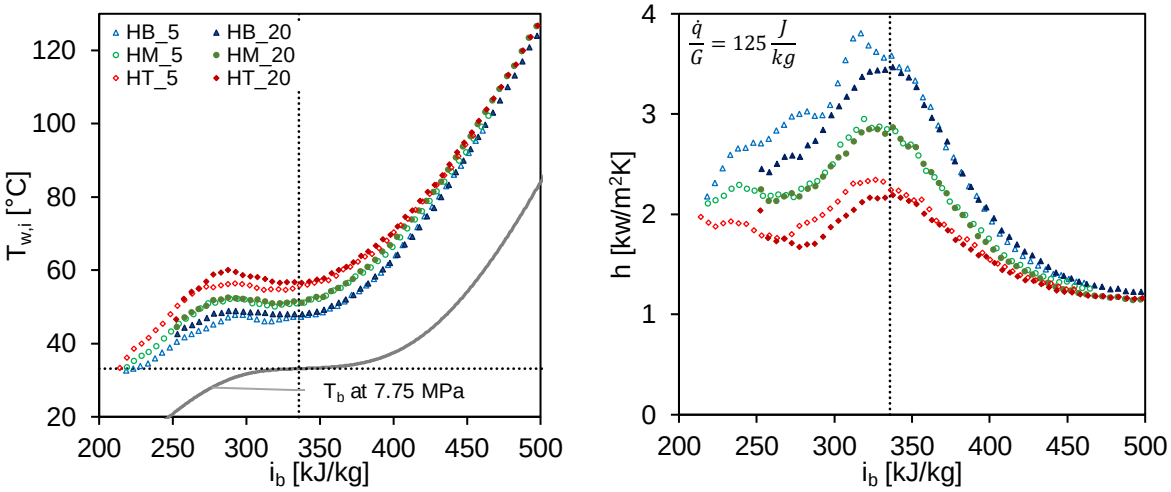

Figure 5: TS1 – d_i= 4mm, G= 400 kg/m^{2}s, q*= 50 kW/m^2

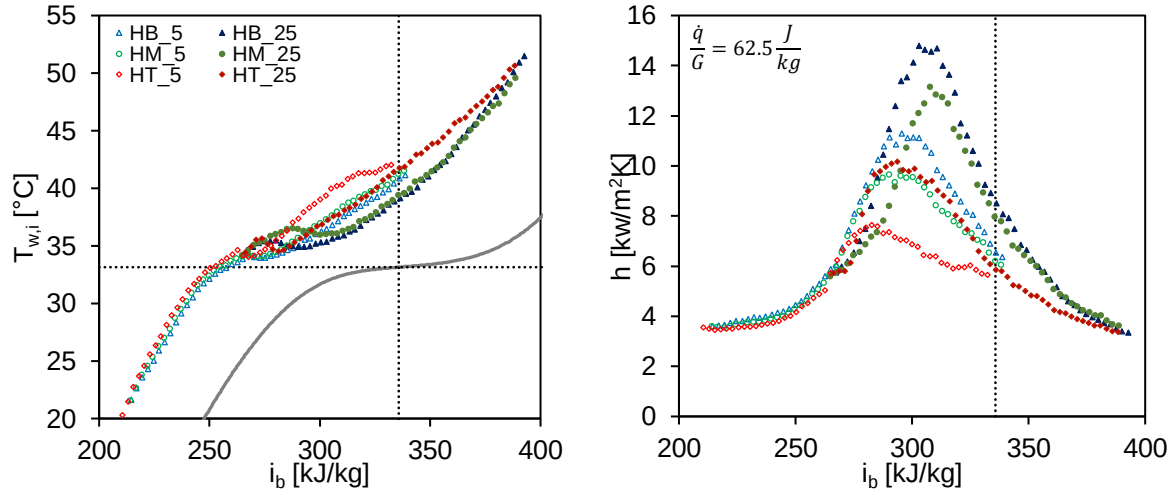

Figure 6: TS2 – d_i= 4mm, G= 800 kg/m^{2}s, q*= 50 kW/m^2

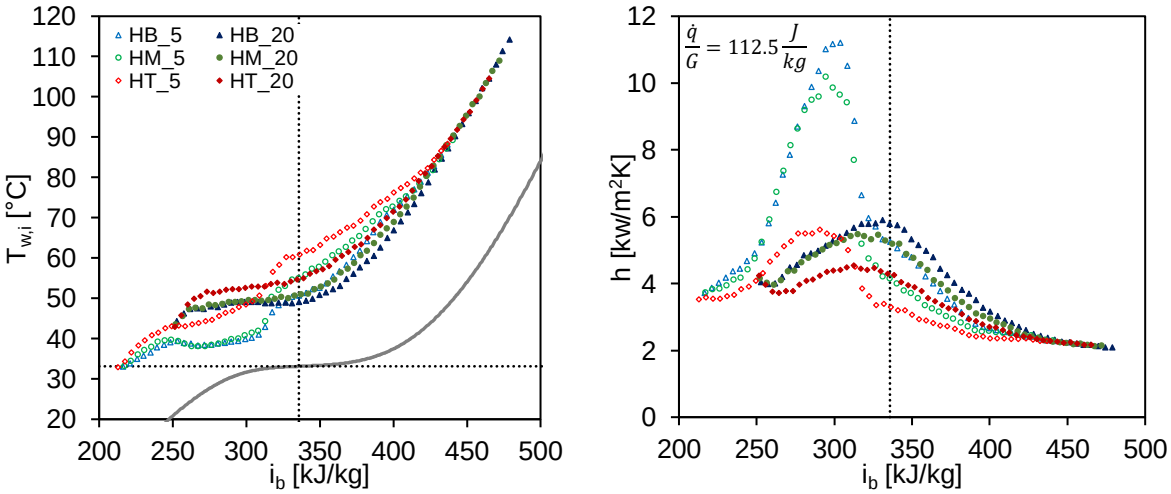

Figure 7: TS3 – d_i= 4mm, G= 800 kg/m^{2}s, q*= 90 kW/m^2

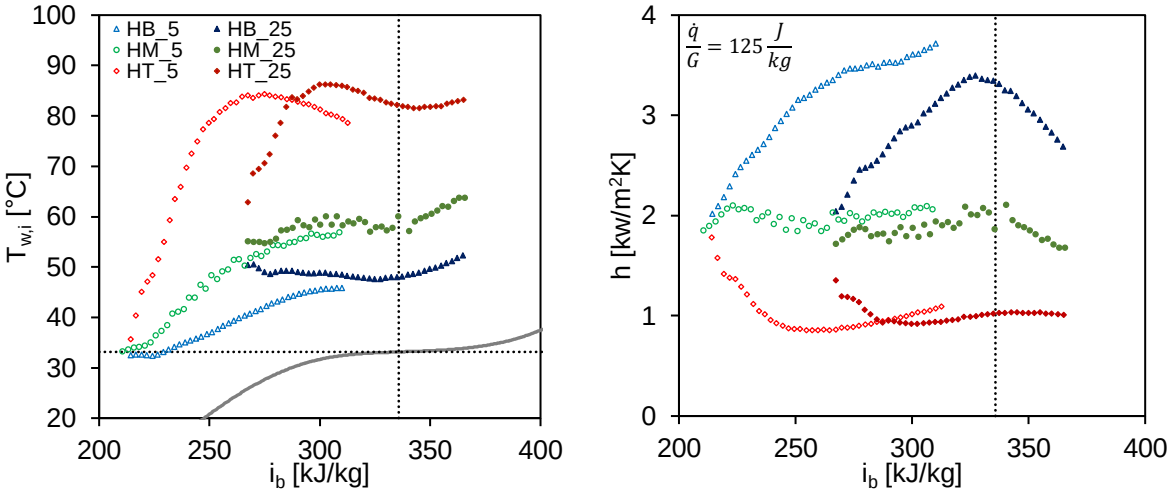

Figure 8: TS4 – d_i= 8mm, G= 400 kg/m^{2}s, q*= 50 kW/m^2

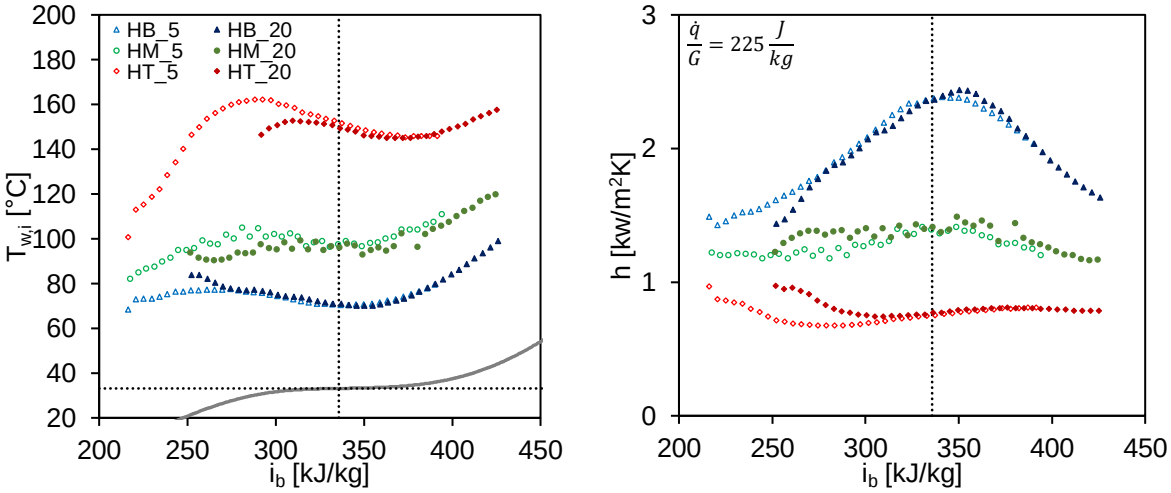

Figure 9: TS5 – d_i= 8mm, G= 400 kg/m^{2}s, q*= 90 kW/m^2

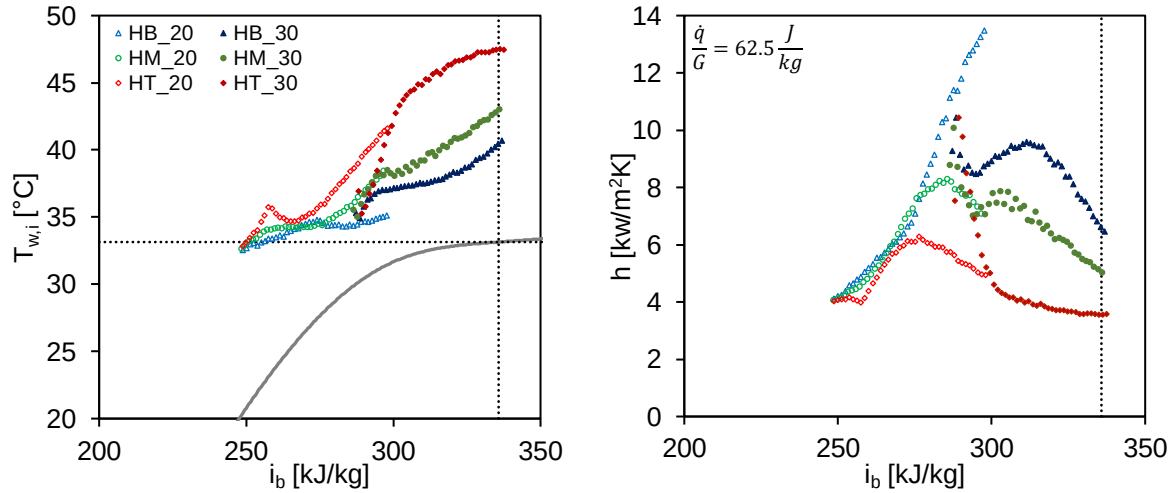

Figure 10: TS6 – d_i= 8mm, G= 800 kg/m^{2}s, q*= 50 kW/m^2

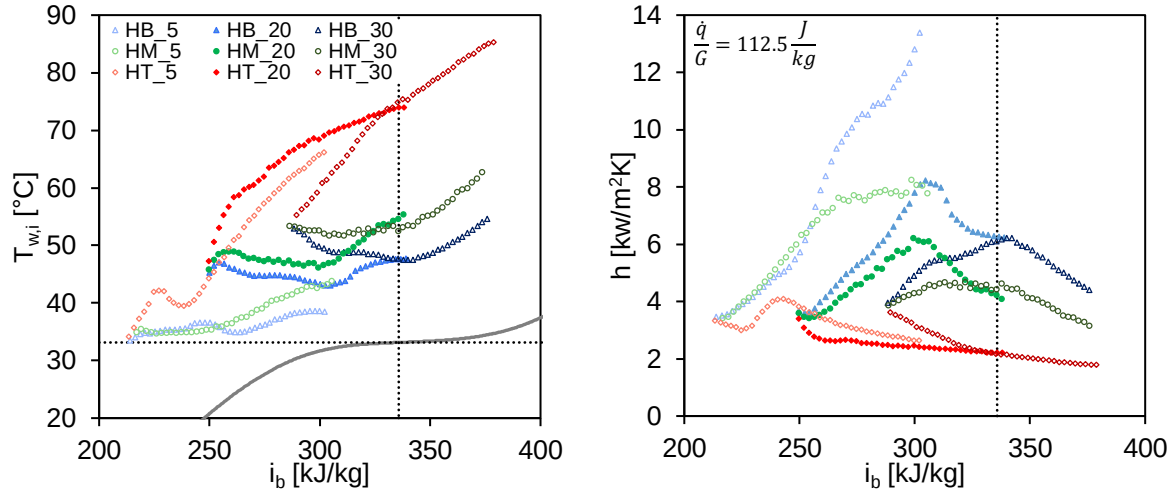

Figure 11: TS7 – d_i= 8mm, G= 800 kg/m^{2}s, q*= 90 kW/m^2

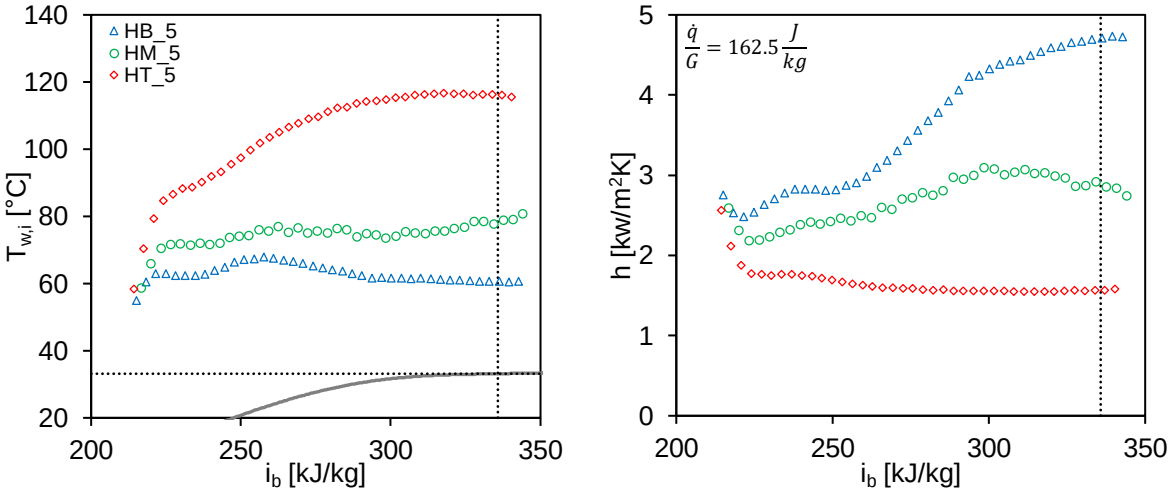

Figure 12: TS8 – d_i= 8mm, G= 800 kg/m^{2}s, q*= 130 kW/m^2

In TS1 (Figure 5) six experiments of the 4 mm pipe were plotted for a heat flux of 50 kW/m^2 and mass flux of 400 kg/m^{2}s leading to a ratio of 125 J/kg. For each sensor position, two experiments with different inlet temperatures of the bulk fluid (5 °C and 20 °C) were carried out. The overlapping of the wall temperature values indicates the end of the thermal inflow length (where the value of the inlet temperature has an influence). The results show a stable temperature stratification. Passing the pseudocritical temperature, the inner wall temperatures start to diverge until they reach the pseudocritical enthalpy. Then they begin to converge again what can be seen by the htc on the right chart. The values converge at an enthalpy of 450 kJ/kg. The maximum temperature difference between the surface at the top and the bottom is approximately 10 K.

For the second test series, (Figure 6) the mass flux has been increased to 800 kg/m^{2}s, so the heat flux to mass flux ratio decreases to 62.5 J/kg. Six experiments were carried out with fluid inlet temperatures of 5 °C and 25 °C. In comparison to the TS1, no clear temperature stratification can be recognized. It is visible that in the range of a mass fluid enthalpy between 300 and 400 kJ/kg in experiments at 5 °C and 25 °C fluid inlet temperature, the values for the temperature at HM and HB are very close together, while the values for HT are always higher. However, an overall scattering of the value profiles (HB, HM and HT) can be seen which converges after a bulk fluid enthalpy of 400 kJ/kg.

By increasing the heat flux up to 90 kW/m^2 in TS3 (Figure 7) the heat flux to mass flux ratio is similar to TS1. Nevertheless, in comparison to TS1, there is no clear temperature stratification. As in TS2, the temperature values of HB and HM are very close to each other, but the values of HT at the pseudo-critical enthalpy are 5-10 K higher. The value profiles converge at a bulk fluid enthalpy of 430 kJ/kg.

The following TSs (Figure 8-Figure 12) show the experimental results for the pipe with 8 mm inner diameter. Beginning with TS4 a mass flux of 400 kg/m^{2}s and a heat flux of 50 kW/m^2 leads to a ratio of 125 J/kg, same as in TS1. The only

difference to TS1 is the inner pipe diameter that leads to higher Reynolds numbers (Table 2). By comparing TS1 and TS4, the temperature stratification in TS4 is more pronounced. The maximum temperature difference between the bottom and the top of the pipe is 45 K. The local temperature peak at the top of the pipe is associated with a deterioration of the htc. This effect cannot be seen at the bottom or the side of the pipe. TS4 can also be compared to TS3 because they have the same Reynolds number and approximately the same value of the heat to mass flux ratio. It shows that the larger inner pipe diameter of 8 mm in TS4 leads to more pronounced temperature stratification.

TS5 (Figure 9) presents the results of six experiments with a heat flux of 90 kW/m^2 and the highest heat to mass flux ratio of 225 J/kg. The results show a very clear temperature stratification with a maximum temperature difference of 90 K between the pipe bottom and the pipe top. The deterioration of heat transfer can be observed more distinctly at the top surface of the pipe.

Figure 10 shows the sixth TS with a mass flux of 800 kg/m^{2}s and a heat flux of 50 kW/m^2, thus, the ratio is 62.5 J/kg, same as in TS2. Despite a higher Reynolds number in TS6 due to a larger diameter, the temperature stratification is more pronounced in the 8 mm pipe, so that the influence of the pipe diameter on the temperature stratification is higher than the influence of the Reynolds number.

With the increase of the heat flux to 90 kW/m^2 in TS7 (Figure 11) and 130 kW/m^2 in TS8 (Figure 12) the temperature stratification became much clearer. For TS7 the maximum temperature difference between the values of HB and HT is approximately 30 K and for TS8 approximately 60 K.

The fluid inlet temperatures of the experiments were chosen in such a way that an overlap of the inner wall temperatures occurs. This makes it possible to quantify the inlet length for a fully developed temperature stratification by a deviation of the inner wall temperatures at the pipe outlet of a previous experiment from the wall temperatures at the pipe inlet of the following experiment (at the next higher inlet fluid temperature of the bulk fluid). The maximum values of HT, HB and HT can be taken for this. For example, for TS5 the HT values of the 20 °C experiment converge to those of the 5 °C experiment after approximately $50d_i$ (10 data points with 40 mm distances correspond to 400 mm inflow length for the 8 mm pipe) and the HB values converge after approximately $30d_i$ (6 data points). Thus, the inlet length for a fully developed temperature stratification can be determined with $50d_i$. For the 30 °C experiment in TS7, this results in an inlet length for a fully developed temperature stratification of $30d_i$ (22 data points of HB).

CONCLUSION

For the investigation of the heat transfer characteristics of sCO_2 in a case where buoyancy effects lead to a temperature stratification, 48 experiments were carried out for two horizontally oriented heated pipes with inner diameters of 4 mm and 8 mm. The outer surface temperatures of the pipes were measured at three different radial pipe positions: The pipe top, the pipe bottom and the pipe side.

The experimental results show that an increased mass flux and Reynolds number with constant heat flux and constant inner diameter leads to reduced temperature differences between the top and the bottom of the pipe. If the ratio of heat to mass flux and the diameter are kept constant while increasing the mass flux and the Reynolds number, no clear temperature stratification appears. With a constant heat to mass flux ratio and Reynolds number, larger pipe diameters lead to more distinct temperature stratification. The results show that the influence of the pipe diameter on the temperature stratification is greater than the influence of the Reynolds number. This set of data can be used for validation of computer codes.

Experiments with higher pressures are planned to investigate the influence of the pressure on the thermal stratification. Furthermore, the results will be analyzed using criteria to determine the influence of buoyancy effects.

NOMENCLATURE

Variables

d	diameter [m] or [mm]
G	mass flux [kg/(m^2 s)]
h	heat transfer coefficient [W/(m^2 K)]
i	specific enthalpy [J/kg]
I	current [A]
L	length [m]
P	electrical power [W]
p	pressure [Pa] or [bar]
$\dot{Q}$	heat transfer rate [W]
$\dot{q}$	heat flux [W/m^2]
Ra	inner roughness [µm]
Re	Reynolds number [-]
s	error [%]
T	temperature [°C] or [K]
U	voltage [V]

Subscripts

b	bulk fluid
el	electric, calculated with el. power
h	heated length
hyd	hydraulic length
i	inner wall
in	inlet fluid conditions
x	local pipe position
o	outer wall
out	outlet fluid conditions
sur	surface of pipe
th	thermal, calculated with bulk fluid
w	pipe-wall

Abbreviations

ATHLET	analysis of thermal-hydraulics of leaks and transients
CHX	compact heat exchanger
DC	direct current
DNS	Direct Numerical Simulation
DP	data point
EUR	European Utility Requirements
HB	pipe bottom
HM	pipe side
HT	pipe top
htc	heat transfer coefficient
HX	heat exchanger
IKE	Institute of Nuclear Technology and Energy Systems
RD	reading accuracy
SCARLETT	Supercritical Carbon Dioxide Loop at IKE Stuttgart
sCO_2	supercritical carbon dioxide
SP	sensor position
TCS	turbo-compressor system
TS	test series

ACKNOWLEDGEMENTS

The presented work was funded by the German Federal Ministry for Economic Affairs and Energy (BMWi. Project no. 1501557) on basis of a decision by the German Bundestag

REFERENCES

[1] Venker, J. (2015). Development and validation of models for simulation of supercritical carbon dioxide Brayton cycles and application to self-propelling heat removal systems in boiling water reactors [Doctoral dissertation]. University of Stuttgart. (10.18419/OPUS-2364).
Society (ANS).

[2] Chu, X. (2016). Direct numerical simulation of heat transfer to supercritical carbon dioxide in pipe flows [Doctoral dissertation]. University of Stuttgart. (10.18419/OPUS-9056).

[3] Dang, C. and Hihara, E. (2004). In-tube cooling heat transfer of supercritical carbon dioxide. Part 1. Experimental measurement. *International Journal of Refrigeration*, *7, pp.* 736–747. (10.1016/j.ijrefrig.2004.04.018).

[4] Liao, S. M. and Zhao, T. S. (2002). Measurements of Heat Transfer Coefficients From Supercritical Carbon Dioxide Flowing in Horizontal Mini/Micro Channels. *Journal of Heat Transfer*, *3, pp.* 413. (10.1115/1.1423906).

[5] Wahl, A.; Mertz, R.; Starflinger, J. (2019, 18-22. August). Experimental investigation of heat transfer in tubes to cool CO_2 near the critical point in horizontal flow orientation [Paper presentation]. *18th International Topical Meeting on Nuclear Reactor Thermal Hydraulics (NURETH-18)*. Portland, OR, USA. American Nuclear Society (ANS).

[6] Xiang, M.; Guo, J.; Huai, X.; Cui, X. (2017). Thermal analysis of supercritical pressure CO_2 in horizontal tubes under cooling condition. *The Journal of Supercritical Fluids, pp.* 389–398. (10.1016/j.supflu.2017.04.009).

[7] Yang, M. (2016). Numerical Study on the Heat Transfer of Carbon Dioxide in Horizontal Straight Tubes under Supercritical Pressure. *PloS one*, *7, pp.* e0159602. (10.1371/journal.pone.0159602).

[8] Yang, C.; Xu, J.; Wang, X.; Zhang, W. (2013). Mixed convective flow and heat transfer of supercritical CO_2 in circular tubes at various inclination angles. *International Journal of Heat and Mass Transfer, pp.* 212–223. (10.1016/j.ijheatmasstransfer.2013.04.033).

[9] Cao, X. L.; Rao, Z. H.; Liao, S. M. (2011). Laminar convective heat transfer of supercritical CO_2 in horizontal miniature circular and triangular tubes. *Applied Thermal Engineering*, *14-15, pp.* 2374–2384. (10.1016/j.applthermaleng.2011.03.038).

[10] Du, Z.; Lin, W.; Gu, A. (2010). Numerical investigation of cooling heat transfer to supercritical CO_2 in a horizontal circular tube. *The Journal of Supercritical Fluids*, *1, pp.* 116–121. (10.1016/j.supflu.2010.05.023).

[11] Yu, S.; Li, H.; Lei, X.; Feng, Y.; Zhang, Y.; He, H.; Wang, T. (2013). Influence of buoyancy on heat transfer to water flowing in horizontal tubes under supercritical pressure. *Applied Thermal Engineering*, *1-2, pp.* 380–388. (10.1016/j.applthermaleng.2013.05.034).

[12] Bazargan, M. and Fraser, D. (2009). Heat Transfer to Supercritical Water in a Horizontal Pipe: Modeling, New Empirical Correlation, and Comparison Against Experimental Data. *Journal of Heat Transfer*, *6, pp.* 61702. (10.1115/1.3082403).

[13] W. Flaig; R. Mertz; J. Starflinger. (2018, 30-31. August). Design, control procedure and start-up of the sCO_2 test facility SCARLETT [Paper presentation]. *2nd European sCO2 Conference 2018*. Essen, Germany. (10.17185/duepublico/46081).

[14] Munson, B. R.; Young, D. F.; Okiishi, T. H. (2006). Fundamentals of fluid mechanics, 5. ed. Wiley.

[15] Theologou, K.; Mertz, R.; Laurien, E.; Starflinger, J. (2019, 19-20. September). An Assessment of the criteria for the onset of heat transfer deterioration with supercritical CO_2 in vertical heated single circular tubes [Paper presentation]. *3rd European supercritical CO2 Conference*. Paris, France. (10.17185/duepublico/48875).

DOI: 10.17185/duepublico/73945
URN: urn:nbn:de:hbz:464-20210330-092057-2